Recessive variants in mitochondrial Complex I nuclear subunits are an underrated cause of optic atrophy

Claudio Fiorini,[1,†] Neringa Jurkute,[2,3,4,†] Alessandra Torraco,[5,†] Chiara La Morgia,[1,6] Daniele Ghezzi,[7,8] Gaia Tioli,[9] Laura Rigobello,[9] Danara Ormanbekova,[1] Alessandro Berghella,[6] Alberto Pietro Pasti,[1] Flavia Palombo,[1] Piero Barboni,[10] Maria Lucia Cascavilla,[10] Federico Sadun,[11] Annamaria De Negri,[12] Enrico Bertini,[13] Olimpia Musumeci,[14] Anna Ardissone,[15] Teresa Rizza,[5] Giancarlo Iarossi,[16] Gabriella Silvestri,[17,18] Salvatore Rossi,[17] Anastasia Altobelli,[5] Antony T. Moore,[2,3] Thomas Cullup,[19] Andrew R. Webster,[2,3] Indran Davagnanam,[20] Michel Michaelides,[2,3] Samantha Malka,[2] Hana Ptackova,[21] Hana Stufkova,[21] Marketa Tesarova,[21] Petra Liskova,[22] Leopold Zeng,[23] Thomas Klopstock,[23,24,25] Robert Kopajtich,[26,27] Christiane Neuhofer,[26,27,28] Holger Prokisch,[26,27,29] Costanza Lamperti,[7] Alfredo A. Sadun,[30,31] Patrick Yu-Wai-Man,[2,3,32,33] Valerio Carelli,[1,6] Francesco Musiani,[9] Luisa Iommarini,[9,‡] Rosalba Carrozzo,[5,‡] Gavin Arno[2,3,34,‡] and Leonardo Caporali[1,‡]

[†,‡]**These authors contributed equally to this work.**

Abstract

Our understanding of the genetic landscape of inherited optic neuropathies has grown significantly over the past decades, and it is now known to involve many genes found in both the nuclear and mitochondrial genomes, exhibiting all possible inheritance patterns. Furthermore, pathogenic variants in nuclear genes of mitochondrial respiratory Complex I (CI) subunits have been identified in some cases of ION, in addition to the more common severe presentation of CI deficiencies, usually with early onset.

We conducted NGS screening of CI genes to identify potential causative variants in patients with optic atrophy, also performing comprehensive clinical assessments, including neuroimaging studies (MRI) and neurological evaluations. Detailed molecular structure modeling was performed

to better evaluate the damaging effects of both novel and previously reported variants in the relevant CI subunits.

We identified and characterized candidate causative variants in 31 patients from 23 unrelated families, with biallelic or hemizygous variants in 11 different nuclear CI-related genes encoding polypeptides involved in the structure of CI, including 3 core subunits (*NDUFS7*, *NDUFV1*, *NDUFV2*), 4 accessory subunits (*NDUFA1*, *NDUFA10*, *NDUFA12*, *NDUFB11*), and 4 assembly factors (*NDUFAF2*, *NDUFAF3*, *NDUFAF4*, *NDUFAF8*). Notably, defects in core CI subunits in this cohort lead to isolated optic atrophy, while defects in accessory CI subunits and assembly factors resulted in a spectrum of phenotypes, from isolated to syndromic optic atrophy. For 12 cases, the subacute onset of vision loss enabled us to associate or confirm novel genes (*NDUFS7*, *NDUFV1*, *NDUFAF2*, *NDUFAF4*, *NDUFAF8*) with the autosomal recessive Leber Hereditary Optic Neuropathy (arLHON) phenotype. Moreover, in the NDUFS7 subunit a partial spatial segregation was noted for missense variants causing either Leigh syndrome or isolated optic atrophy, hinting at possible disease-specific molecular defects.

Our case series broadens the genetic spectrum of inherited optic neuropathies, emphasizing the crucial role of nuclear CI genes in its pathogenesis. The arLHON phenotype emerges as linked to numerous nuclear CI genes for which an insidious onset of optic atrophy is also reported, and in some cases the same variant may underlie both phenotypes. Overall, we highlight the possibly so far underestimated prevalence of CI nuclear subunits in the molecular diagnosis of ION, prompting to include all CI-related genes in the standard diagnostic screening.

Author affiliations:

1 IRCCS Istituto delle Scienze Neurologiche di Bologna, Programma di Neurogenetica, 40139 Bologna, Italy

2 Moorfields Eye Hospital NHS Foundation Trust, London EC1V 2PD, UK

3 Institute of Ophthalmology, University College London, London EC1V 9EL, UK

4 The National Hospital for Neurology and Neurosurgery, Queen Square, University College London Hospitals NHS Foundation Trust, London WC1N 3BG, UK

5 Laboratory of Medical Genetics, Translational Cytogenomics Research Unit, Bambino Gesù Children's Hospital IRCCS, 00146 Rome, Italy

6 Department of Biomedical and Neuromotor Sciences (DIBINEM), University of Bologna, 40139 Bologna, Italy

7 Fondazione IRCCS Istituto Neurologico Carlo Besta, Unit of Medical Genetics and Neurogenetics, 20126 Milan, Italy

8 Department of Pathophysiology and Transplantation, University of Milan, 20126 Milan, Italy

9 Department of Pharmacy and Biotechnology (FABIT), University of Bologna, 40126 Bologna, Italy

10 IRCCS Ospedale San Raffaele, 20132 Milan, Italy

11 Ospedale Oftalmico Roma, 00136 Rome, Italy

12 Azienda Ospedaliera San Camillo-Forlanini, 00152 Rome, Italy

13 Research Unit of Neuromuscular and Neurodegenerative Disorders, Bambino Gesù Children's Hospital IRCCS, 00146 Rome, Italy

14 Department of Experimental and Clinical Medicine, University of Messina, 98122 Messina, Italy

15 Fondazione IRCCS Istituto Neurologico Carlo Besta, Child Neurology Unit, 20133 Milan, Italy

16 Ophthalmology Unit, Bambino Gesù Children's Hospital IRCCS, 00165 Rome, Italy

17 Department of Neuroscience, Università Cattolica del Sacro Cuore-Sede di Roma, 00168 Rome, Italy

18 Neurology Unit, Fondazione Policlinico Universitario Agostino Gemelli IRCCS, Largo A Gemelli, 00168 Rome, Italy

19 North Thames Genomic Laboratory Hub, Great Ormond Street Hospital, Guilford St, London WC1N 3BH, UK

20 Department of Brain Repair and Rehabilitation, University College London Institute of Neurology, Faculty of Brain Sciences, UCL, London WC1N 3AR, UK

21 Department of Paediatrics and Inherited Metabolic Disorders, First Faculty of Medicine, Charles University and General University Hospital in Prague, 121 08 Prague, Czech Republic

22 Department of Ophthalmology, First Faculty of Medicine, Charles University and General University Hospital in Prague, 121 08 Prague, Czech Republic

23 Friedrich-Baur-Institute, Department of Neurology, University Hospital, Ludwig-Maximilians University, 81377 Munich, Germany

24 German Center for Neurodegenerative Diseases, 81377 Munich, Germany

25 Munich Cluster for Systems Neurology (SyNergy), 81377 Munich, Germany

26 Institute of Human Genetics, Computational Health Center, Helmholtz Zentrum München, 85764 Neuherberg, Germany

27 Institute of Human Genetics, School of Medicine, Technical University of Munich, 81675 Munich, Germany

28 Department of Clinical Human Genetics, University Medical Center Regensburg, 93053 Regensburg, Germany

29 German Center for Child and Adolescent Health (DZKJ), partner site Munich, 80636 Munich, Germany

30 Doheny Eye Institute, Pasadena, CA 91103, USA

31 Department of Ophthalmology, David Geffen School of Medicine, UCLA, Los Angeles, CA 90095, USA

32 John van Geest Centre for Brain Repair and MRC Mitochondrial Biology Unit, Department of Clinical Neurosciences, University of Cambridge, Cambridge CB2 0XY, UK

33 Cambridge Eye Unit, Addenbrooke's Hospital, Cambridge University Hospitals NHS Foundation Trust, Cambridge CB2 0QQ, UK

34 Greenwood Genetic Center, Greenwood, South Carolina 29646, USA

Correspondece to: Leonardo Caporali

Ospedale Bellaria, Via Altura 3, 40139 Bologna, Italy

E-mail leonardo.caporali@isnb.it

Introduction

Inherited optic neuropathies (ION) include two major entities: the first is maternally inherited Leber hereditary optic neuropathy (LHON) (MIM #535000), typically caused by homoplasmic mitochondrial DNA (mtDNA) point mutations. The second is autosomal dominant optic atrophy (ADOA) (MIM #165500), which is predominantly caused by heterozygous pathogenic variants in the *OPA1* gene encoded by nuclear DNA (nDNA).[1–3] Both affect respiratory complex I (CI, EC 7.1.1.2), the largest enzymatic complex of the mitochondrial electron transfer system which is composed in humans by 45 unique subunits. Those are assembled in functionally and evolutionarily distinctive modules, namely the NADH dehydrogenase module (N), the quinone binding module (Q) and the proton pumping module (P), the latter being further subdivided in two proximal submodules (ND1- and ND2-submodules) and two distal submodules (ND4- and ND5-submodules).[4] Indeed, the three most common mtDNA pathogenic variants associated with LHON affect genes (*MT-ND1*, *MT-ND4*, *MT-ND6*) encoding CI core subunits, directly impairing the complex catalytic function.[1] In contrast, *OPA1* variants associated with ADOA do not directly affect CI, as its enzymatic activity remains normal,[5] but instead influence CI-driven oxidative phosphorylation efficiency likely due to disrupted mitochondrial dynamics and *cristae* morphology.[6,7]

In addition to the classic clinical manifestation of isolated optic atrophy (OA), both LHON and ADOA can also manifest with syndromic phenotypes described under the broader LHON and ADOA "plus" groups.[1–3] These phenotypes may arise from more severe and rarer mtDNA pathogenic variants for LHON plus,[8–10] or from specific missense pathogenic variants, mostly affecting the GTPase domain of the OPA1 protein, in the case of ADOA plus.[11,12]

Beyond the well-established associations of mtDNA-LHON and *OPA1*-ADOA, the genetic landscape of optic neuropathies has expanded to include several other nDNA-encoded genes or *loci* (also identified as OPA2-16), which underly both autosomal dominant, recessive and X-linked inheritance patterns.[13,14] In this broader context of newly identified ION-related genes, the role of CI dysfunction in the pathogenesis of optic nerve pathology remains of utmost importance.[15–17]

Overall, an increasing number of nuclear CI-related genes have recently been recognized as genetic causes of autosomal recessive LHON (arLHON), including core subunits, accessory subunits, and assembly factors (i.e. *NDUFS2*, *NDUFS7*, *NDUFA12*, *NDUFAF2*, *NDUFAF5*).[18–22] Furthermore, a gene involved in CI N module turnover and quality control, *DNAJC30*, has emerged as a relatively frequent cause of arLHON (LHONAR1, MIM #619382) undistinguishable from LHON caused by mtDNA pathogenic variants.[23,24] Finally, *TMEM126A,* a gene responsible for isolated or syndromic OA with recessive inheritance (OPA7, MIM #612989),[25–27] has been found to encode a key factor for CI biogenesis, interacting with the ND4 module.[28–30]

Finally, it is important to note that most pathogenic variants in nuclear subunits of CI are typically associated with CI deficiency and severe early-onset phenotypes, mainly attributable to autosomal recessive Leigh Syndrome (LS) or Leigh-like Syndrome (LLS) spectrum.[31] While the clinical presentation of LS is highly variable and complex, visual impairment due to OA is a recurrent feature in about 15 % of patients, though ophthalmic evaluation may not always be performed, especially in very young and severely affected patients.[32]

In the current study, we identified a significant role of biallelic defects in CI nuclear-encoded subunits as a mechanism of ION, also including arLHON, while such findings have previously been recognized in only a handful of cases.[14] Moreover, in this international cohort we describe patients with an OA plus or LLS presentation, harboring variants in otherwise scarcely reported CI subunits. Finally, we present evidence that a structural approach considering subunit location as well as specific aminoacidic substitutions can shed some light on the phenotypic and genetic diversity observed.

Materials and methods

Clinical evaluation

Clinical assessments included best-corrected visual acuity (BCVA) by Snellen charts extrapolated to decimal values, color vision tests, slit-lamp biomicroscopy, tonometry, color fundus photography, optical coherence tomography (OCT; Cirrus, Carl Zeiss Meditec Inc., Dublin, CA, USA; DRI Triton, Topcon, Tokyo, Japan or SPECTRALIS spectral-domain-OCT, Heidelberg

Engineering GmbH, Heidelberg, Germany), automated visual field test (Humphrey Field Analyzer, protocol Sita Standard 30-2/24-2; Zeiss, San Leandro, CA or M-700, Medmont International, Vermont, Australia). OCT protocols included the evaluation of peripapillary retinal nerve fiber layer (pRNFL) thickness (3.4 acquisition protocol).

Genetic investigations

The genetic testing for each patient was approved by ethical committees of respective institutes and authorized by informed consent. Sequencing of nuclear genes was performed after complete mtDNA sequencing that excluded the presence of pathogenic variants. In the different institutions, NGS screenings were performed as follows: target gene panel for mitochondrial disorders at IRCCS Istituto Neurologico Carlo Besta, Milano, IT (Families B, H, I, L) and at Charles University and General University Hospital, Prague, CZ (Family M); clinical exome at Moorfields Eye Hospital, London, UK (Families C and T) and at IRCCS Ospedale Pediatrico Bambino Gesù, Roma, IT (Families D, G, H, J); whole exome sequencing at IRCCS Istituto delle Scienze Neurologiche di Bologna, Bologna, IT (Families A, E, K, G, N, O, P, R, S) and at TUM Klinikum, Munich, DE (Family U); and whole genome sequencing at Moorfields Eye Hospital, London, UK (Families F, Q, V, W).

Methods used in NGS data generation and processing, including variant filtering and prioritization are reported in the Supplementary Methods. The details of all NGS screenings performed and quality metrics obtained are reported in Supplementary Table 1.

Variant classification was performed according to ACMG guidelines, using the REVEL score of meta-prediction for the application of PP3/BP4 criteria, then also adapted through the use of targeted modeling (see "In silico prediction of pathogenicity" paragraph).[33–35]

In silico prediction of pathogenicity

To unravel the functional role of newly identified variants associated with OA and to search for possible functional differences between them and those previously reported in the literature as causative for LS/LLS, we conducted a comprehensive *in silico* analysis. The current literature (updated to February 2025) was searched to produce a list of pathogenic variants in the genes found in the current study. For each article we collected PMID number, genetic variants, main

phenotype, and information about the proband and alleles (summarized in Supplementary Table 2).

Firstly, for each variant we used two different tools to calculate the impact of missense variants on protein folding by calculating the ΔΔG induced by every variant, namely DynaMut2[36] and DUET[37], with the latter utilizing predictions made by mCSM[38] and SDM[39]. These tools have been chosen because they performed the best in benchmarking experiments among the publicly available web services.[40] We considered the variants as impacting on protein folding only when both predictors coherently showed a value of ΔΔG that exceeds (in positive or negative) the root mean square error (RMSE) indicated for each predictor, that is ±1.02 kcal/mol and ±0.98 kcal/mol for DynaMut2 and DUET respectively. When the prediction was not consistent for the two tools, we considered the effect on that variant as uncertain. The structures used to exploit these tools were PDB id 5XTD for human CI,[41] and those predicted by AlphaFold 3 (AF3)[42] for NDUFAF2, NDUFAF3, NDUFAF4 and NDUFAF8. For these predicted structures, we performed the ΔΔG calculation only if the segment affected by the variant had a predicted Local Distance Difference Test score plDDT > 70, corresponding to a high confidence of the prediction. Lastly, we mapped the amino acid affected by variants on human CI structure and predicted structures, performed *in silico* mutagenesis and, when possible, we investigated their involvement in the formation of protein-protein interaction (PPI) and the characteristics of the interfaces by using PDBePISA.[43] Mitochondrial targeting sequences (MTS) were identified using MTSviewer[44] and variants reported on the 3D structure predicted by AF3. For NDUFAF3 N-terminal, which is not modelled as an α-helix by AF3, we predicted the secondary structure using JPred4[45] and generated a structural model of the first 32 amino acids using UCSF ChimeraX 1.8.[46] The same software was used for the visual inspections and the modelling of the variants, exploiting the *swapaa* tool.

For the adjustment of ACMG PP3/BP4 criteria of variants described in our cases, we combined evidence from the two ΔΔG modeling tools with two sequence-based tools that provide prediction about structural impact of amino acid changes, namely Alpha Missense (AM)[47] and PrimateAI-3D (PAI-3D)[48]. The calibrated prediction scores (ranging from 0 to 1) and pathogenicity prediction categories (likely benign, ambiguous, or likely pathogenic for AM, benign or pathogenic for PAI-3D) are reported in Supplementary Tables 5-7. When all the approaches for structural evaluation were concordant in identifying a variant as damaging, we applied an upgraded PP3 criterion as

reported in Supplementary Table 3. The same algorithm was applied for variants affecting the MTS, taking its specific modeling in substitution to ΔΔG prediction.

Quantitative Proteomics

TMT-labelled mass spectrometry was performed at the BayBioMS core facility of the Technical University of Munich described by Kopajtich et al. with two minor modifications.[49] Peptide fractionation was carried out using high pH reversed phase instead of trimodal mixed-mode chromatography and TMT-labelling was carried out using TMT 11-plex instead of TMT 10-plex reagent. Quantification of NDUFAF5 protein and complex I subunits has been carried out in a single TMT batch of 11 samples.

Data normalization and expression outlier analysis was conducted using PROTRIDER[50] in a dataset of n=815 fibroblast samples.

Results

Variants in multiple CI nuclear subunits are associated with optic neuropathy

We identified biallelic or hemizygous candidate pathogenic genotypes in 11 different genes encoding subunits of respiratory CI across 31 patients from 23 families. These patients had no putative causative variants in the mitochondrial genome or in other nuclear genes associated with OA (Fig. 1, Table 1). The identified variants were located in 3 core subunits (*NDUFS7*, *NDUFV1*, *NDUFV2*), 4 accessory subunits (*NDUFA1*, *NDUFA10*, *NDUFA12, NDUFB11*), and 4 assembly factors (*NDUFAF2*, *NDUFAF3*, *NDUFAF4*, *NDUFAF8*). Overall, based on ACMG criteria, we classified 10 variants as pathogenic, 6 variants as likely pathogenic, and 4 variants as VUS (Supplementary Table 3). For these latter missense variants, additional evidence coming from recurrence in independent families and *in silico* modeling were integrated in the ACMG classification.

The combined prevalence of CI-related nuclear genes (as listed in Supplementary Methods) in ION was assessed on a subset of the cohort, screened at Italian and German diagnostic centers. A total of 836 probands were subjected to WES with a yield of 45% cases where genetics findings were reported. This cohort included 38 cases harboring variants in CI nuclear genes, increasing the total diagnostic yield by 5% and representing 10% of all solved cases.

Patients exhibited a broad spectrum of clinical manifestations, ranging from isolated OA to OA 'plus', which included features such as nystagmus, Wolff-Parkinson-White (WPW) syndrome, hearing impairment, intellectual disability, seizures, cerebellar ataxia, peripheral axonal neuropathy, and LLS with basal ganglia and brainstem abnormalities (Fig. 2, Tables 2 and 3, Supplementary Table 4). The OA onset was either insidious during childhood or presented acutely/subacutely in young adulthood, resembling the clinical course of LHON (Tables 2 and 3, Supplementary Table 4). Pharmacological treatments for OA included idebenone, CoQ10, riboflavin, and ubidecarenone at variable dosages. Visual improvement was variable, with only three patients out of 13 showing some degree of response to idebenone treatment (Supplementary Table 4).

We evaluated structural properties and pathogenicity prediction for missense variants identified in our cohort, as well as for those previously reported in the literature, also associated with other phenotypes (Supplementary Table 2). Specifically, we combined structure-based prediction tools such as Alpha Missense and PrimateAI-3D with an estimation of impact on protein folding (ΔΔG) to add a line of pathogenicity evidence to a commonly used meta-prediction tool (REVEL). Full data regarding pathogenicity prediction and ΔΔG values are reported in Supplementary Tables 5-7 and discussed together with mapping and *in silico* mutagenesis for each affected polypeptide.

Defects in core CI subunits lead to isolated optic atrophy

Eight patients from seven families (A-G) carried previously unreported variants in *NDUFS7*, *NDUFV1*, or *NDUFV2*, encoding core subunits of CI (Fig. 3A). These patients typically exhibited isolated OA, with either an insidious onset during childhood or an acute/subacute onset similar to LHON in young adulthood (16-25 years range, Table 2). At last clinical evaluation, no significant new symptoms were reported, except for nystagmus in the proband of Family A and Wolff-Parkinson-White (WPW) syndrome in the proband of Family E. Additionally, a subclinical

hyperintensity of the posterior part of the cervical spinal cord was noted in the proband of Family G, carrying *NDUFV2* variants, likely attributable to vitamin B12 deficiency (Tables 2 and 3).

NDUFS7 (NM_024407.5)

The proband from Family A was found to carry both a missense variant c.223C>T p.(R75C) and a small indel c.559_564delinsTAGAT p.(A187*). The homozygous variant c.298C>T p.(R100C) was detected in affected individuals from families B and C, while the homozygous variant c.313C>T p.(R105C) was found in affected individuals from families D and E, making *NDUFS7* the most commonly affected gene in our case series. The missense variants p.(R100C) and p.(R105C) were predicted as pathogenic by AM and PAI-3D, while p.(R75C) was classified as ambiguous by AM. The ΔΔG values for these variants were inconsistently predicted by DynaMut2 and DUET, thus being classified as uncertain for their potential impact of the subunit folding. The five variants previously reported in the literature are predicted as likely pathogenic by AM, while PAI-3D classifies all of them as pathogenic except for p.(P144L) and p.(R145H), which nevertheless show high pathogenicity scores (Supplementary Table 5). Among these variants, p.(L126F), p.(R145H) and p.(R168S) associated with LS were also predicted to have an impact on protein folding based on their ΔΔG values. The most striking difference between variants previously reported and those described here is their location within the 3D structure of CI. Indeed, the first ones grouped together close to the Fe-S cluster N2, associated with the ubiquinone (coenzyme Q10, CoQ10) binding site, while the latter are situated in the N-terminal of the subunit (Fig. 3B). Specifically, p.(R100) and p.(R105) are positioned peripherally in an external region of the subunit and are involved in the formation of PPI interfaces with NDUFS2, NDUFS8, NDUFA7 and NDUFA12. These are distinct from the remaining variants, which mediate the interactions between NDUFS7 and NDUFS3, NDUFA9 and ND3 (Supplementary Table 8). Notably, p.R100 forms a hydrogen bond with p.E208 of NDUFS2 using its side chain (distance 3.29Å), meaning this interaction could be disrupted by the variants identified in families B and C, while the side chain of p.R105 is H-bonded with p.I82 of NDUFS8 (distance 3.89Å), which may be compromised by the variant found in families D and E. The only subunit interacting with NDUFS7 using residues from both cohorts is ND1, which forms a PPI interface involving both p.R75 (Family A) and p.R105 (families D and E), as well as p.P144 which is also mutated in a published OA case.[21]

NDUFV1 (NM_007103.4)

The proband from Family F carried the homozygous variant c.1156C>A p.(R386S), at a known mutational hotspot of *NDUFV1,* where pathogenic variants p.(R386C) and p.(R386H) have previously been described in several LS patients following the first published cases.[51,52] Among the subunits studied, *NDUFV1* harbors the highest number of pathogenic variants, with 28 linked to LS in the literature, that are all are predicted as pathogenic by AM, while PAI-3D classifies 17/28 variants as pathogenic and 11/28 as benign (Supplementary Table 5). Some of these variants are predicted to impact protein folding and are generally spread across the protein, though they tend to cluster around specific regions, such as the FMN-binding site and the Fe-S clusters N1a and N3.

In particular, p.R386 is located on the subunit surface within the four-helix bundle of the NDUFV1 subunit and plays a role in forming PPI interface with NDUFS1 (Fig. 3C, Supplementary Table 8). Moreover, it is part of an extended H-bond network involving its guanidino tail and NDUFV1 residues p.G380, p.Q381, p.T383, and NDUFS1 residue p.Q178. Residue p.S386 also forms a π-stacking interaction with the side chains (Supplementary Fig. 1). These interactions could be disrupted when p.R386 is replaced by a shorter amino acid, such as serine, cysteine or histidine. However, it remains unclear how the specific serine substitution would cause a milder phenotype compared to its substitution with cysteine or histidine. No clear biochemical differences can be inferred from the available data, aside from the proximity of residue 386 to the Fe-S cluster N3, which may undergo positional shifts in the presence of cysteine, potentially affecting its function.

NDUFV2 (NM_021074.5)

The proband from Family G was found to carry compound heterozygous c.163T>G p.(F55V) and c.674G>A p.(C225Y) variants. Both of these variants, along with the five variants reported in the literature, are all predicted to be pathogenic (Fig. 3D). Two of these are likely to affect protein folding, namely p.(F55V) found in the present cohort and p.(E194K) already reported in literature (Supplementary Table 5). The two OA-associated variants are located at distant sites, with no apparent mutational hotspots also considering the LS-associated variants (Fig. 3D). NDUFV2 forms several PPIs with NDUFV1, NDUFV3, NDUFS1, NDUFS4 and NDUFS6 (Supplementary Table 8). Among these interactions, only the interface with NDUFV1 contains mutated residues, specifically p.C225 (mutated in Family G) and p.T232 (reported in the literature).

Defects in accessory CI subunits lead to a spectrum from isolated to syndromic optic atrophy

Ten patients from eight families (Families H-O) carried hemizygous variants in *NDUFA1* or *NDUFB11* genes, or biallelic variants in *NDUFA10* or *NDUFA12*, encoding accessory subunits of CI. In all patients, OA began during childhood, except for family N, which exhibited a LHON-like onset. Most patients, except families M and N, showed signs of syndromic disease, including hearing impairment, intellectual disability, and movement disorders associated with basal ganglia abnormalities, seizures and cerebellar ataxia. Bilateral pallidal and dentate hyperintensity was observed in only one patient (Family H) (Fig.2E-F). Cerebellar atrophy was reported in 2 cases (Family J and L). One patient (Family K) also had multiple sclerosis (MS). (Tables 2 and 3)

NDUFA1 (NM_004541.4)

The probands from families H and I both carried the novel missense variant c.28T>C p.(S10P); while the proband of Family J carried the missense variant c.55C>T p.(P19S), which has been reported in two published cases of LS.[53,54] This subunit contains four variants previously reported in the literature, along with two novel variants identified in our cohort for which pathogenicity predictions by AM and PAI-3D are uncertain, as well as their impact on ΔΔG (Supplementary Table 6). Focusing on the variants identified in this study, p.(P19S) is predicted to be pathogenic and to affect protein folding, while p.(S10P) is generally reported as benign. However, this variant was found in two independent families, with no alleles present the gnomAD v4.1 dataset, supporting its pathogenicity. When mapping the variants in the 3D structure model, OA-associated variants are located in the N-terminal helix of NDUFA1, where the p.(G8R) variant (reported in the literature) also resides (Fig. 4B). The other LS-associated variants are located in the loop connecting the two main α-helices. Notably, residues from the N-terminal region are involved in forming a PPI with ND1, similarly to NDUFS7. We hypothesize that the p.(P19S) variant could result in the formation of a longer transmembrane helix that, in turn, could impact the protein folding, as predicted by high variations in ΔΔG values. However, the effect of p.(S10P) variant remains difficult to define, even if proline insertion into α-helices is often disruptive.

NDUFA10 (NM_004544.4)

The proband from families K and L carried the homozygous in-frame deletion c.233_235del p.(A78del). This variant has been previously reported in a case of LS, in *trans* with c.296G>A p.(G99E).[55] Two siblings from Family M harbored the homozygous missense variant c.1009C>T p.(R337C); this genotype has been previously reported in a patient with ataxia, hypotonia and developmental regression.[56] In total, five missense variants have been reported in this subunit in LS cases, including the p.(R337C) variant identified in the present cohort, highlighting that other genetic factors likely modulate the clinical phenotype in these patients (Supplementary Table 6, Fig. 4C). While the in-frame deletion of residue p.A78 can be predicted as pathogenic for the lack of the single amino acid, missense variants are variably predicted by AM and PAI-3D. However, p.(R337C) shows an impact on protein folding with a significant divergent value of ΔΔG (Supplementary Table 6). Additionally, in the 3D structure p.G99 and p.R337 are in close proximity and are involved in PPI interfaces with NDUFC1, NDUFC2 and ND2 (Fig. 4C and Supplementary Table 8). Specifically, the p.(R337C) variant could induce a reduction in steric bulk affecting the protein folding, while p.(G99E) may form a salt bridge with p.R337, thus impacting on the flexibility of the loop containing p.G99.

NDUFA12 (NM_018838.5)

Two siblings from Family N were found to be homozygous for the novel stop-gain variant c.69T>G p.(Y23*). To date, only loss-of-function (LoF) variants have been identified in this subunit. Nevertheless, a complex phenotypic spectrum characterizes *NDUFA12* cases and even the arLHON phenotype as observed in our cases has been reported.[19,57]

NDUFB11 (NM_019056.7)

The proband from Family O carried the hemizygous in frame deletion c.276_278del p.(F93del), which was first described as a recurrent variant in patients with syndromic sideroblastic anemia due to CI deficiency (with myopathy, lactic acidosis, optic atrophy).[58] Three missense variants in this subunit have been reported in the literature (Supplementary Table 6), and they are distributed along the entire length of the protein without clear hotspots (Fig. 4D). From the protein interaction perspective, NDUFB11 interacts with 11 subunits, including ND4 through the residues p.F93 and

p.P110 (Supplementary Table 7), suggesting these residues play a critical role in the assembly of CI.

Defects in assembly CI factors lead to a spectrum from isolated to syndromic optic atrophy

Thirteen patients from eight families (Families P-W) carried compound heterozygous variants in *NDUFAF2*, *NDUFAF3*, *NDUFAF4* or *NDUFAF8*, encoding assembly factors of CI. Six patients out of 13, carrying *NDUFAF2, NDUFAF4* or *NDUFAF8* variants, showed a LHON-like phenotype (Tables 2 and 3). All three patients from Family P and Q, carrying variants in *NDUFAF2,* showed OA and peripheral axonal neuropathy, while the single patient harboring *NDUFAF3* variants showed LLS with basal ganglia hyperintensity (Fig.2C-D) and motor delay. The phenotype associated with variants in *NDUFAF4* was characterized by isolated OA in all three patients, as observed also for five out of six patients with *NDUFAF8* variants; the remaining proband also exhibited cerebellar ataxia and nystagmus. One of the patients carrying *NDUFAF4* variants who presented with insidious OA also suffered at the age of 17 years a LHON-like visual loss.[59] Additionally, basal ganglia/brainstem abnormalities, white matter changes, and cerebellar atrophy were reported in most cases. The *in-silico* analyses were performed for these polypeptides based on the structures generated by AF3 (Fig. 5 and Supplementary Table 7).

NDUFAF2 (NM_174889.5)

Two affected siblings from Family P carried the novel missense variant c.95A>G p.(Y32C) and the frameshift variant c.148del p.(R50Efs*3), which was recently reported in *trans* with c.139C>T, p.(R47*) in a patient with an LHON-like phenotype.[20] The proband from family Q carried the homozygous nonsense variant c.114C>G, p.(Y38*), which was known from a patient with LS.[60] The amino acid change p.Y32C is the first missense pathogenic variant described and lies in a well modelled antiparallel β-sheet (Fig. 5A). This variant is predicted as pathogenic by both AM and PAI-3D, highlighting a possible detrimental effect on protein function.

NDUFAF3 (NM_199069.2)

The proband from Family R carried the novel variant c.5C>A, p.(A2D) and the c.489_490del p.(G164Sfs*29) already reported in a LS case.[61] The p.(A2D) variant is located at the N-terminal

of NDUFAF3, in contrast to the five other variants reported in the literature, associated with LS and predicted as pathogenic, affecting amino acids in the well-modelled globular C-terminal portion of the protein (Fig. 5B). The N-terminal (aa 1-31) is predicted by MTSviewer as a canonical MTS but is not well modelled by AF3. However, when the secondary structure is predicted using JPred4, p.(A2D) amino acid change is found to disrupt the positively charged surface of the N-terminal amphipathic α-helix, thus possibly impacting the protein import.

NDUFAF4 (NM_014165.4)

The proband from Family S carried the novel biallelic variants c.224del p.(P75Lfs*7) and c.413T>C p.(I138T), with the latter variant also found in the homozygous state in the two affected siblings from Family T. The p.I138T variant is predicted as pathogenic and is likely to destabilize the protein folding (Supplementary Table 7). This amino acid lies in a well-modelled globular domain of NDUFAF4 (Fig. 5C), clearly distant from those LS-associated reported in literature affecting the N-terminal, which are ambiguous in terms of pathogenicity prediction, but may affect the import of this assembly factor.

NDUFAF8 (NM_001086521.2)

The siblings from Family U carried the homozygous novel missense variant c.44T>G p.(L15R), while the probands from families V and W carried the homozygous deep intronic variant c.195+271C>T p.?. This latter variant was already described in two independent families affected by LS, in compound heterozygosity with pathogenic alleles, and it was confirmed to induce transcript decay.[62] The AF3 model is moderately accurate for the N-terminal α-helix where the p.L15 residue is located, however the change is predicted to be part of the MTS introducing a positive charge on the hydrophobic side of the amphipathic α-helix (Fig. 5D), possibly affecting NDUFAF8 import into the mitochondria.

To validate the impact of the p.L15R variant at the protein level, we performed quantitative proteomics on fibroblasts derived from individual II-4 in a batch of 11 samples. NDUFAF8 protein was not detected in the whole TMT 11-plex batch, not allowing us to directly evaluate the variant effect. However, we observed a strong reduction of NDUFAF5 protein (fold change: 0.18, Supplementary Fig. 2A), another CI assembly factor known to require NDUFAF8 for its

stability.[62] Moreover, a moderate reduction of CI protein level (mean fold change: 0.73) was observed, indicating an impaired assembly pathway (Supplementary Fig. 2B).

Variants of uncertain significance of mtDNA in recessive OA cases

It is now established that a clinical phenotype of LS can result from digenic variants in CI subunits encoded in both nuclear and mitochondrial genomes.[63] To explore this phenomenon in our cohort, we also investigated the affected individuals' mtDNA sequence background (Supplementary Table 9). No imbalance in major haplogroups frequency was observed over the 23 Families of the cohort, where we observed haplogroup C (*n*=1), H (*n*=8), J (*n*=3), M (*n*=2), N (*n*=1), R0 (*n*=1), U (*n*=4), V (*n*=1), X (*n*=2). A total of six families harbored missense variants in mitochondrial CI genes, namely *MT-ND1*, *MT-ND2*, *MT-ND3*, *MT-ND5*, *MT-ND6*. Among those, the proband of Family I carried three different variants in CI genes, including the m.3394T>C/*MT-ND1* already associated with several phenotypes, especially a population-specific LHON.[64] Two more families carried missense variants in the ATPase complex, namely m.9025G>A/*MT-ATP6* in Family A, previously reported in a LS case,[65] and m.8555T>C/*MT-ATP6* in Family N.

Discussion

This study describes a series of 31 affected individuals from 23 families in whom OA was the primary phenotype, with some cases showing additional symptoms and pathogenic variants in nuclear-encoded CI subunits. Overall, we associate for the first time the arLHON phenotype with variants in *NDUFAF4* and *NDUFAF8* genes, and we consolidate *NDUFS7*, *NDUFV1*, and *NDUFAF2* variants as causative for arLHON, while previously reported in single families.[20,21] Furthermore, isolated or plus OA was found for the first time in *NDUFV2*, *NDUFA1*, *NDUFA10*, and *NDUFAF3* families, for which only a single report of arLHON existed for a patient carrying *NDUFA10* variants.[66]

In all patients, previous genetic screening excluded the involvement of mtDNA or other optic neuropathies-related genes. Clinically, a subset of these patients experienced a subacute loss of vision resembling LHON, while others had an insidious onset of OA in childhood. It remains poorly understood what drives the difference in disease onset, the subacute deterioration of visual

acuity in adolescence or young-adult age hallmarking LHON, as opposed to the more insidious onset in childhood, as typically seen for *OPA1*-DOA. However, as already well described, even in LHON pedigrees with mtDNA common variants both kinds of disease onset may be seen.[67] While OA was an isolated feature in about half of the patients, others exhibited broader involvement of the central and peripheral nervous systems, with manifestations ranging from peripheral neuropathy and sensory neural ataxia to nystagmus, neurosensory hearing impairment, basal ganglia lesions, and LLS features. Extra-neurological features included megaloblastic anemia and WPW syndrome, whereas lactic acidosis was a frequent laboratory finding. These findings greatly expand the genetic landscape of recessive OA, including arLHON, suggesting that LS/LLS and OA/arLHON are the two extremes of a phenotypic spectrum with variable severity seen more frequently than previously thought.

To understand the possible genotype-phenotype correlation, we categorized the CI subunits carrying the pathogenic variants according to their function in the complex, with three main groups including core subunits, accessory subunits, and assembly factors. The variants in the CI core subunits (*NDUFS7*, *NDUFV1*, and *NDUFV2*) were associated with isolated OA in six out of eight patients, with only one case also having upbeat nystagmus and another one WPW syndrome. Half of these patients can be categorized as arLHON/arLHON plus based on disease onset and progression.

It is important to note that among the 14 core subunits of CI, three are the most affected by primary LHON variants, namely ND1, ND4 and ND6, suggesting that functions carried out by the catalytically competent enzyme core may be phenotypically linked to subacute vision loss characterizing LHON. Congruently with this observation, the first report describing arLHON found biallelic variants in *NDUFS2* which is a core subunit.[17] Indeed, core subunits are responsible for the redox activity and proton translocation,[30] as well as for the recently proposed function of mitochondrial Na^+/H^+ exchanger,[68] which seems to be involved in the pathogenetic mechanism of the classic LHON mutation m.11778G>A/MT-ND4.

Defects in CI accessory subunits may also have a pronounced impact on the complex structure and function, similar to what is observed for the core subunits.[69] However, the pathogenic variants affecting accessory subunits (*NDUFA1*, *NDUFA10*, *NDUFA12*, *NDUFB11*) were more frequently associated with OA plus (in five out of ten patients) and LLS phenotype (in one patient). Only two

families carrying *NDUFA10* and *NDUFA12* variants presented with isolated OA. This may be related to the role of accessory subunits, most of which are known to be necessary for human CI assembly and stability.[69] In this frame, variants in accessory subunits may induce clinical phenotypes which are more similar to those caused by variants in assembly factors. Indeed, in the latter category (*NDUFAF2*, *NDUFAF3*, *NDUFAF4*, *NDUFAF8),* we observed both isolated and plus OA phenotypes for the 13 patients, including one LLS case. For example, both families harboring variants in *NDUFAF4* showed isolated OA, whereas all three *NDUFAF2* patients had multisystemic involvement. Given their role in the CI assembly, predicting their functional impact *in silico* is challenging due to varying levels of partially assembled sub-complexes and residual CI activity, that should be demonstrated experimentally.

The core subunits described for our cohort are all located in the matrix portion of the complex, specifically in module N (NDUFV1 and NDUFV2) and module Q (NDUFS7), which also interacts with the accessory subunits NDUFA1 and NDUFA12 that are connected to the membrane arm.[70] The assembly factors in which we identified pathogenic variants are variously involved in CI assembly. In fact, according to complexome profiling studies NDUFAF3 and NDUFAF4 are necessary for the early connection of the Q module to ND1, NDUFAF2 is involved in the late maturation of the Q module, while NDUFAF8 contributing to early stabilization of NDUFS7 together with NDUFAF5.[62,71] This latter polypeptide, lacking from our cohort, has recently been found mutated in two cases showing OA/arLHON.[22,72] Since NDUFS2 and DNAJC30 are as well part of, or involved in, stability of the peripheral arm of CI, this portion of the complex appears to be a hotspot for recessive OA variants.

Our structural analysis also uncovered a possible segregation of variants either linked to LS or OA in different parts of NDUFS7, the subunit most frequently affected in our OA cohort, that is located at the connection of peripheral and membrane arms of CI and is involved in the formation of the CoQ binding site.[73] Notably, the variants identified here clustered around the N-terminal region and formed PPI with subunits such as NDUFS2, NDUFA12, and ND1, which have been commonly linked to OA and LHON/arLHON phenotypes in literature.

Using up-to-date structural prediction tools, like Alpha Missense and PrimateAI-3D, together with ΔΔG investigations, we were able to apply more precise criteria for pathogenicity prediction (PP3) of missense variants according to ACMG. Therefore, for 6 out of 13 missense variants we found

evidence supporting a damaging role of the aminoacidic change, where REVEL meta-prediction was unable to assess the effect. Notably, we identified two variants affecting the properties of the MTS of NDUFAF3 and NDUFAF8, proving experimentally for the latter that the pathogenic variant impact on NDUFAF8 abundance into the mitochondria and affect CI assembly. The only variant lacking support to a pathogenic role based on structural evidence is p.(S10P) in NDUFA1, which would require further functional investigations. In-depth modeling could therefore help in the improvement of ACMG criteria assessment beyond the commonly available prediction and meta-prediction tools' results.

An important observation to highlight is the clinical variability that can occur with the same pathogenic variant in different individuals. For example, in two siblings homozygous for the *NDUFA10* p.(R337C) variant we observed isolated OA, whereas a previously published case with the same amino acid change was reported with multisystemic involvement.[56] Even within the same family we observed discordant phenotypes, as in the case of Family V carrying the recurrent *NDUFAF8* c.195+271C>T intronic variant, here associated with either isolated or plus arLHON phenotype. The phenotypic variability may be influenced by multiple factors, including genetic modifiers in both mitochondrial and nuclear genomes, as well as exposure to environmental factors as well documented for LHON.[74]

We also note the presence of mtDNA variants with possible functional impact but without clear-cut pathogenicity in some of the patients from our cohort. A plausible hypothesis is that mtDNA variants could act synergistically with nDNA variants to exacerbate disease severity. However, an epistatic interaction might also counterbalance the effect of amino acid changes in nuclear subunits. Predicting the interaction between multiple specific variants remains challenging and would likely require advanced molecular dynamics modeling, at least for those affecting the same protein complexes, or *in-vitro*/*in-vivo* functional validation. For instance, the m.3394T>C/MT-ND1 variant, identified in Family I, was reported to interact with m.11778G>A/MT-ND4, increasing LHON penetrance of LHON,[75] and with haplogroup and environmental, [76] becoming benign or pathogenic depending on the context.

Moreover, in Family A proband we detected both biallelic *NDUFS7* variants and the m.9025G>A variant in *MT-ATP6* reported as pathogenic, with yeast validation in support.[77] However, it is relatively frequent in healthy controls (i.e. 45/56418 homoplasmic cases in gnomAD v4.1) and its

role in disease modulation is unclear. Strikingly, a few reports attributed a pathogenic role to *MT-ATP6* variants in LHON patients.[65,78] However, noticeably these probands were singleton cases without any evidence of maternal inheritance, raising doubt that as evidenced by the 3 cases found in this study, the real molecular defect resides in nuclear genes.

In conclusion, our study demonstrates that OA, whether LHON-like or with insidious early onset, is frequently consequent upon biallelic or hemizygous variants in nuclear genes involved in CI structure and assembly. Moreover, OA can be part of the LS/LLS spectrum more commonly known for the nuclear CI genes, but can also occur as an isolated feature. Our study prompts a change in the diagnostic algorithm for ION patients, that should now always include the screening of all known CI-related genes, as, although individually rare, their combined prevalence can be comparable to other well-established ION genes, as reported by other studies.[16,17,66] Finally, these patients may benefit from treatment with idebenone, following appropriate dosage and standard protocols like those used for LHON. Idebenone, in its reduced form, can bypass CI and transfer electrons from NADH directly to respiratory complex III, thus restoring downstream electron transport chain and oxidative phosphorylation.[79] In this respect, any CI defect may be partially corrected through the drug's mechanism of action.

Data availability

The authors confirm that the data supporting the findings of this study are available within the article and its supplementary material.

Raw data were generated in each participating center. Derived data supporting the findings of this study are available from the corresponding author on request.

Acknowledgements

We thank all participating patients and their relatives.

This research was made possible through access to data in the National Genomic Research Library, which is managed by Genomics England Limited (a wholly owned company of the Department of Health and Social Care). The National Genomic Research Library holds data provided by patients

and collected by the NHS as part of their care and data collected as part of their participation in research. The National Genomic Research Library is funded by the National Institute for Health Research and NHS England. The Wellcome Trust, Cancer Research UK and the Medical Research Council have also funded research infrastructure.

Funding

PYWM is supported by an Advanced Fellowship Award (NIHR301696) from the UK National Institute of Health Research (NIHR). PYWM also receives funding from the Rosetrees Trust (PGL23/100048), Fight for Sight (UK), the Isaac Newton Trust (UK), Moorfields Eye Charity (GR001376), the Addenbrooke's Charitable Trust, the National Eye Research Centre (UK), the International Foundation for Optic Nerve Disease (IFOND), the NIHR as part of the Rare Diseases Translational Research Collaboration, the NIHR Cambridge Biomedical Research Centre (NIHR203312), and the NIHR Biomedical Research Centre based at Moorfields Eye Hospital NHS Foundation Trust and UCL Institute of Ophthalmology (NIHR203322). This research was supported by LifeArc under grant no. 10748. LifeArc is a charity registered in England and Wales under no. 1015243 and in Scotland under no. SC037861. The views expressed are those of the author(s) and not necessarily those of the NHS, the NIHR or the Department of Health.

LC is supported by the Italian Ministry of Health grant GR-2016-02361449. VC is supported by Italian Ministry of Health funding "Ricerca Corrente". VC is also supported by NextGenerationEU (NGEU) and funded by the Ministry of University and Research (MUR), National Recovery and Resilience Plan (NRRP), project MNESYS (PE0000006) – A Multiscale integrated approach to the study of the nervous system in health and disease (DN. 1553 11.10.2022).

GT and LI are supported by the European Union - NextGenerationEU, Mission 4, Component 2, CUP B93D21010860004.

PL is supported by the Czech Ministry of Health AZV NU22-07-00614 and by Charles University and General University Hospital in Prague UNCE/24/MED/022 and SVV 2600631.

HP is supported by the German Federal Ministry of Education and Research (BMBF) and Horizon2020 through the E-Rare project GENOMIT (01GM1920A, B), by the German Center for Child and Adolescent Health (DZKJ) under the funding code 01GL2406B.

Competing interests

The authors report no competing interests.

Supplementary material

Supplementary material is available at *Brain* online.

References

1. Carelli V, Ross-Cisneros FN, Sadun AA. Mitochondrial dysfunction as a cause of optic neuropathies. *Prog Retin Eye Res*. 2004;23:53-89. doi:10.1016/j.preteyeres.2003.10.003

2. Yu-Wai-Man P, Griffiths PG, Chinnery PF. Mitochondrial optic neuropathies – Disease mechanisms and therapeutic strategies. *Prog Retin Eye Res*. 2011;30(2):81-114. doi:10.1016/J.PRETEYERES.2010.11.002

3. Carelli V, La Morgia C, Yu-Wai-Man P. Mitochondrial optic neuropathies. *Handb Clin Neurol*. 2023;194:23-42. doi:10.1016/B978-0-12-821751-1.00010-5

4. Ugalde C, Vogel R, Huijbens R, van der Heuvel B, Smeitink J, Nijtmans L. Human mitochondrial complex I assembles through the combination of evolutionary conserved modules: a framework to interpret complex I deficiencies. *Hum Mol Genet*. 2004;13(20):2461-2472. doi:10.1093/HMG/DDH262

5. Mayorov VI, Lowrey AJ, Biousse V, Newman NJ, Cline SD, Brown MD. Mitochondrial oxidative phosphorylation in autosomal dominant optic atrophy. *BMC Biochem*. 2008;9(1). doi:10.1186/1471-2091-9-22

6. Zanna C, Ghelli A, Porcelli AM, et al. OPA1 mutations associated with dominant optic atrophy impair oxidative phosphorylation and mitochondrial fusion. *Brain*. 2008;131(Pt 2):352-367. doi:10.1093/BRAIN/AWM335

7. Cogliati S, Frezza C, Soriano ME, et al. Mitochondrial cristae shape determines respiratory chain supercomplexes assembly and respiratory efficiency. *Cell*. 2013;155(1):160-171. doi:10.1016/J.CELL.2013.08.032

8. Jun AS, Brown MD, Wallace DC. A mitochondrial DNA mutation at nucleotide pair 14459 of the NADH dehydrogenase subunit 6 gene associated with maternally inherited Leber hereditary optic neuropathy and dystonia. *Proc Natl Acad Sci U S A*. 1994;91(13):6206-6210. doi:10.1073/PNAS.91.13.6206

9. Valentino ML, Barboni P, Rengo C, et al. The 13042G --> A/ND5 mutation in mtDNA is pathogenic and can be associated also with a prevalent ocular phenotype. *J Med Genet*. 2006;43(7). doi:10.1136/JMG.2005.037507

10. Vacchiano V, Caporali L, La Morgia C, et al. The m.3890G>A/MT-ND1 mtDNA rare pathogenic variant: Expanding clinical and MRI phenotypes. *Mitochondrion*. 2021;60:142-149. doi:10.1016/J.MITO.2021.08.007

11. Amati-Bonneau P, Valentino ML, Reynier P, et al. OPA1 mutations induce mitochondrial DNA instability and optic atrophy "plus" phenotypes. *Brain*. 2008;131(Pt 2):338-351. doi:10.1093/BRAIN/AWM298

12. Yu-Wai-Man P, Griffiths PG, Gorman GS, et al. Multi-system neurological disease is common in patients with OPA1 mutations. *Brain*. 2010;133(Pt 3):771-786. doi:10.1093/brain/awq007

13. Newman NJ, Yu-Wai-Man P, Biousse V, Carelli V. Understanding the molecular basis and pathogenesis of hereditary optic neuropathies: towards improved diagnosis and management. *Lancet Neurol*. 2023;22(2):172-188. doi:10.1016/S1474-4422(22)00174-0

14. Lenaers G, Beaulieu C, Charif M, Gerber S, Kaplan J, Rozet JM. Autosomal recessive Leber hereditary optic neuropathy, a new neuro-ophthalmo-genetic paradigm. *Brain*. 2023;146(8):3156-3161. doi:10.1093/BRAIN/AWAD131

15. Maresca A, Carelli V. Molecular mechanisms behind inherited neurodegeneration of the optic nerve. *Biomolecules*. 2021;11(4):1-32. doi:10.3390/biom11040496

16. Rocatcher A, Desquiret-Dumas V, Charif M, et al. The top 10 most frequently involved genes in hereditary optic neuropathies in 2186 probands. *Brain*. 2023;146(2):455-460. doi:10.1093/BRAIN/AWAC395

17. Fiorini C, Ormanbekova D, Palombo F, et al. The Italian reappraisal of the most frequent genetic defects in hereditary optic neuropathies and the global top 10. *Brain*. 2023;146(9):E67-E70. doi:10.1093/BRAIN/AWAD080

18. Gerber S, Ding MG, Gérard X, et al. Compound heterozygosity for severe and hypomorphic NDUFS2 mutations cause non-syndromic LHON-like optic neuropathy. *J Med Genet*. 2017;54(5):346-356. doi:10.1136/JMEDGENET-2016-104212

19. Magrinelli F, Cali E, Braga VL, et al. Biallelic Loss-of-Function NDUFA12 Variants Cause a Wide Phenotypic Spectrum from Leigh/Leigh-Like Syndrome to Isolated Optic Atrophy. *Mov Disord Clin Pract*. 2022;9(2):218-228. doi:10.1002/mdc3.13398

20. Chen IH, Chang HH, Chiu HI, Cheng HC, Wang AG. Autosomal Recessive Leber Hereditary Optic Neuropathy in a Patient With a Novel NDUFAF2 Compound Heterozygous Mutation. *J Neuroophthalmol*. Published online November 3, 2023. doi:10.1097/WNO.0000000000002029

21. Chermakani P, Gowri P, Kumar SM, Sundaresan P. Exploring mito-nuclear genetic factors in Leber's hereditary optic neuropathy: insights from comprehensive profiling of unique cases. *EXCLI J*. 2023;22:1077-1091. doi:10.17179/EXCLI2023-6297

22. Chen J, Wu Y, Yu S, Wan X, Gong Y, Sun X. Cognitive Impairment in Phenotypic Leber Hereditary Optic Neuropathy Caused by Mutation in Nuclear Gene NDUFAF5. *Journal of Neuro-Ophthalmology*. 2024;44(1):E20-E22. doi:10.1097/WNO.0000000000001760

23. Stenton SL, Sheremet NL, Catarino CB, et al. Impaired complex I repair causes recessive Leber's hereditary optic neuropathy. *J Clin Invest*. 2021;131(6). doi:10.1172/JCI138267

24. Stenton SL, Tesarova M, Sheremet NL, et al. DNAJC30 defect: a frequent cause of recessive Leber hereditary optic neuropathy and Leigh syndrome. *Brain*. 2022;145(5):1624-1631. doi:10.1093/brain/awac052

25. Hanein S, Perrault I, Roche O, et al. TMEM126A, encoding a mitochondrial protein, is mutated in autosomal-recessive nonsyndromic optic atrophy. *Am J Hum Genet*. 2009;84(4):493-498. doi:10.1016/J.AJHG.2009.03.003

26. Meyer E, Michaelides M, Tee LJ, et al. Nonsense mutation in TMEM126A causing autosomal recessive optic atrophy and auditory neuropathy. *Mol Vis*. 2010;16:650-664. http://www.molvis.org/molvis/v16/a74

27. La Morgia C, Caporali L, Tagliavini F, et al. First TMEM126A missense mutation in an Italian proband with optic atrophy and deafness. *Neurol Genet*. 2019;5(3). doi:10.1212/NXG.0000000000000329

28. D'Angelo L, Astro E, De Luise M, et al. NDUFS3 depletion permits complex I maturation and reveals TMEM126A/OPA7 as an assembly factor binding the ND4-module intermediate. *Cell Rep*. 2021;35(3). doi:10.1016/J.CELREP.2021.109002

29. Formosa LE, Reljic B, Sharpe AJ, et al. Optic atrophy-associated TMEM126A is an assembly factor for the ND4-module of mitochondrial complex I. *Proc Natl Acad Sci U S A*. 2021;118(17). doi:10.1073/PNAS.2019665118

30. Poerschke S, Oeljeklaus S, Cruz-Zaragoza LD, et al. Identification of TMEM126A as OXA1L-interacting protein reveals cotranslational quality control in mitochondria. *Mol Cell*. 2024;84(2):345-358.e5. doi:10.1016/J.MOLCEL.2023.12.013

31. Fiedorczuk K, Sazanov LA. Mammalian Mitochondrial Complex I Structure and Disease-Causing Mutations. *Trends Cell Biol*. 2018;28(10):835-867. doi:10.1016/j.tcb.2018.06.006

32. Ardissone A, Bruno C, Diodato D, et al. Clinical, imaging, biochemical and molecular features in Leigh syndrome: a study from the Italian network of mitochondrial diseases. *Orphanet J Rare Dis*. 2021;16(1). doi:10.1186/s13023-021-02029-3

33. Richards S, Aziz N, Bale S, et al. Standards and guidelines for the interpretation of sequence variants: a joint consensus recommendation of the American College of Medical Genetics and Genomics and the Association for Molecular Pathology. *Genet Med*. 2015;17(5):405-424. doi:10.1038/gim.2015.30

34. Ioannidis NM, Rothstein JH, Pejaver V, et al. REVEL: An Ensemble Method for Predicting the Pathogenicity of Rare Missense Variants. *Am J Hum Genet*. 2016;99(4):877-885. doi:10.1016/J.AJHG.2016.08.016

35. Pejaver V, Byrne AB, Feng BJ, et al. Calibration of computational tools for missense variant pathogenicity classification and ClinGen recommendations for PP3/BP4 criteria. *The American Journal of Human Genetics*. 2022;109(12):2163-2177. doi:10.1016/J.AJHG.2022.10.013

36. Rodrigues CH, Pires DE, Ascher DB, David Ascher CB, eduau unimelb. DynaMut2: Assessing changes in stability and flexibility upon single and multiple point missense mutations. *Protein Science*. 2021;30(1):60-69. doi:10.1002/PRO.3942

37. Pires DEV, Ascher DB, Blundell TL. DUET: a server for predicting effects of mutations on protein stability using an integrated computational approach. *Nucleic Acids Res*. 2014;42(W1):W314-W319. doi:10.1093/NAR/GKU411

38. Pires DEV, Rodrigues CHM, Ascher DB. mCSM-membrane: predicting the effects of mutations on transmembrane proteins. *Nucleic Acids Res*. 2020;48(W1):W147-W153. doi:10.1093/NAR/GKAA416

39. Worth CL, Preissner R, Blundell TL. SDM--a server for predicting effects of mutations on protein stability and malfunction. *Nucleic Acids Res*. 2011;39(Web Server issue). doi:10.1093/NAR/GKR363

40. Benevenuta S, Birolo G, Sanavia T, Capriotti E, Fariselli P. Challenges in predicting stabilizing variations: An exploration. *Front Mol Biosci*. 2023;9:1075570. doi:10.3389/FMOLB.2022.1075570/BIBTEX

41. Guo R, Zong S, Wu M, Gu J, Yang M. Architecture of Human Mitochondrial Respiratory Megacomplex I2III2IV2. *Cell*. 2017;170(6):1247-1257.e12. doi:10.1016/J.CELL.2017.07.050

42. Abramson J, Adler J, Dunger J, et al. Accurate structure prediction of biomolecular interactions with AlphaFold 3. *Nature*. 2024;630(8016):493-500. doi:10.1038/s41586-024-07487-w

43. Evgeny K. Crystal contacts as nature's docking solutions. *J Comput Chem*. 2010;31(1):133-143. doi:10.1002/JCC.21303

44. Bayne AN, Dong J, Amiri S, Farhan SMK, Trempe JF. MTSviewer: A database to visualize mitochondrial targeting sequences, cleavage sites, and mutations on protein structures. *PLoS One*. 2023;18(4):e0284541. doi:10.1371/JOURNAL.PONE.0284541

45. Drozdetskiy A, Cole C, Procter J, Barton GJ. JPred4: a protein secondary structure prediction server. *Nucleic Acids Res*. 2015;43(W1):W389-W394. doi:10.1093/NAR/GKV332

46. Goddard TD, Huang CC, Meng EC, et al. UCSF ChimeraX: Meeting modern challenges in visualization and analysis. *Protein Sci*. 2018;27(1):14-25. doi:10.1002/PRO.3235

47. Cheng J, Novati G, Pan J, et al. Accurate proteome-wide missense variant effect prediction with AlphaMissense. *Science (1979)*. 2023;381(6664). doi:10.1126/SCIENCE.ADG7492/ASSET/A671A6AA-91B7-4005-A07D-8E8494F9632F/ASSETS/IMAGES/LARGE/SCIENCE.ADG7492-F5.JPG

48. Gao H, Hamp T, Ede J, et al. The landscape of tolerated genetic variation in humans and primates. *Science (1979)*. 2023;380(6648). doi:10.1126/SCIENCE.ABN8197/SUPPL_FILE/SCIENCE.ABN8197_MDAR_REPRODUCIBILITY_CHECKLIST.PDF

49. Scheller IF, Klaproth-Andrade D, Loipfinger S, et al. PROTRIDER: Protein abundance outlier detection from mass spectrometry-based proteomics data with a conditional autoencoder. *bioRxiv*. Published online February 5, 2025:2025.02.01.636024. doi:10.1101/2025.02.01.636024

50. Kopajtich R, Smirnov D, Stenton SL, et al. Integration of proteomics with genomics and transcriptomics increases the diagnostic rate of Mendelian disorders. *medRxiv*. Published online July 3, 2021:2021.03.09.21253187. doi:10.1101/2021.03.09.21253187

51. Breningstall GN, Shoffner J, Patterson RJ. Siblings with leukoencephalopathy. *Semin Pediatr Neurol*. 2008;15(4):212-215. doi:10.1016/J.SPEN.2008.10.013

52. Vilain C, Rens C, Aeby A, et al. A novel NDUFV1 gene mutation in complex I deficiency in consanguineous siblings with brainstem lesions and Leigh syndrome. *Clin Genet*. 2012;82(3):264-270. doi:10.1111/J.1399-0004.2011.01743.X

53. Uehara N, Mori M, Tokuzawa Y, et al. New MT-ND6 and NDUFA1 mutations in mitochondrial respiratory chain disorders. *Ann Clin Transl Neurol*. 2014;1(5):361. doi:10.1002/ACN3.59

54. Miyauchi A, Osaka H, Nagashima M, et al. Leigh syndrome with spinal cord involvement due to a hemizygous NDUFA1 mutation. *Brain Dev*. 2018;40(6):498-502. doi:10.1016/J.BRAINDEV.2018.02.007

55. Yahya V, Spagnolo F, Di Maggio G, et al. Juvenile-onset dystonia with spasticity in Leigh syndrome caused by a novel NDUFA10 variant. *Parkinsonism Relat Disord*. 2022;104:85-87. doi:10.1016/J.PARKRELDIS.2022.10.016

56. Monies D, Abouelhoda M, Assoum M, et al. Lessons Learned from Large-Scale, First-Tier Clinical Exome Sequencing in a Highly Consanguineous Population. *The American Journal of Human Genetics*. 2019;104(6):1182-1201. doi:10.1016/j.ajhg.2019.04.011

57. Torraco A, Nasca A, Verrigni D, et al. Novel NDUFA12 variants are associated with isolated complex I defect and variable clinical manifestation. *Hum Mutat*. 2021;42(6):699-710. doi:10.1002/humu.24195

58. Lichtenstein DA, Crispin AW, Sendamarai AK, et al. A recurring mutation in the respiratory complex 1 protein NDUFB11 is responsible for a novel form of X-linked sideroblastic anemia. *Blood*. 2016;128(15):913-917. doi:10.1182/BLOOD-2016-05-719062

59. Barboni P, Battista M, Brotto L, et al. Recurrence of Visual Loss in Recessive Leber Hereditary Optic Neuropathy: New Paradigm. *J Neuroophthalmol*. 2025;45(1). doi:10.1097/WNO.0000000000002117

60. Hoefs SJG, Dieteren CEJ, Rodenburg RJ, et al. Baculovirus complementation restores a novel NDUFAF2 mutation causing complex I deficiency. *Hum Mutat*. 2009;30(7). doi:10.1002/HUMU.21037

61. Walker MA, Miranda M, Allred A, Mootha VK. On the dynamic and even reversible nature of Leigh syndrome: Lessons from human imaging and mouse models. *Curr Opin Neurobiol*. 2022;2022:80-90. doi:10.1016/j.conb.2021.09.006

62. Alston CL, Veling MT, Heidler J, et al. Pathogenic Bi-allelic Mutations in NDUFAF8 Cause Leigh Syndrome with an Isolated Complex I Deficiency. *Am J Hum Genet*. 2020;106(1):92-101. doi:10.1016/J.AJHG.2019.12.001

63. Blickhäuser B, Stenton SL, Neuhofer CM, et al. Digenic Leigh syndrome on the background of the m.11778G>A Leber hereditary optic neuropathy variant. *Brain*. 2024;147(6):1967-1974. doi:10.1093/brain/awae057

64. Ji F, Sharpley MS, Derbeneva O, et al. Mitochondrial DNA variant associated with Leber hereditary optic neuropathy and high-altitude Tibetans. *Proc Natl Acad Sci U S A*. 2012;109(19):7391-7396. doi:10.1073/PNAS.1202484109/-/DCSUPPLEMENTAL/PNAS.201202484SI.PDF

65. López-Gallardo E, Emperador S, Solano A, et al. Expanding the clinical phenotypes of MT-ATP6 mutations. *Hum Mol Genet*. 2014;23(23):6191-6200. doi:10.1093/HMG/DDU339

66. Zheng Y, Wang P, Li S, et al. Clinical and genetic landscape of optic atrophy in 826 families: insights from 50 nuclear genes. *Brain*. 2024;139(4):16-17. doi:10.1093/BRAIN/AWAE324

67. Barboni P, La Morgia C, Cascavilla ML, et al. Childhood-Onset Leber Hereditary Optic Neuropathy-Clinical and Prognostic Insights. *Am J Ophthalmol*. 2023;249:99-107. doi:10.1016/J.AJO.2022.12.014

68. Hernansanz-Agustín P, Morales-Vidal C, Calvo E, et al. A transmitochondrial sodium gradient controls membrane potential in mammalian mitochondria. *Cell*. 2024;187(23):6599-6613.e21. doi:10.1016/J.CELL.2024.08.045

69. Stroud DA, Surgenor EE, Formosa LE, et al. Accessory subunits are integral for assembly and function of human mitochondrial complex I. *Nature*. 2016;538(7623):123-126. doi:10.1038/nature19754

70. Guerrero-Castillo S, Baertling F, Kownatzki D, et al. The Assembly Pathway of Mitochondrial Respiratory Chain Complex I. *Cell Metab*. 2017;25(1):128-139. doi:10.1016/J.CMET.2016.09.002

71. van der Ven AT, Cabrera-Orefice A, Wente I, et al. Expanding the phenotypic and biochemical spectrum of NDUFAF3-related mitochondrial disease. *Mol Genet Metab*. 2023;140(3). doi:10.1016/J.YMGME.2023.107675

72. Mansukhani SA, Mehta DG, Renaud DL, Whealy MA, Chen JJ, Bhatti MT. Nuclear DNA Mutation Causing a Phenotypic Leber Hereditary Optic Neuropathy Plus. *Ophthalmology*. 2021;128(4):628-631. doi:10.1016/J.OPHTHA.2020.09.011

73. Kampjut D, Sazanov LA. The coupling mechanism of mammalian respiratory complex I. *Science*. 2020;370(6516). doi:10.1126/SCIENCE.ABC4209

74. Caporali L, Maresca A, Capristo M, et al. Incomplete penetrance in mitochondrial optic neuropathies. *Mitochondrion*. 2017;36:130-137. doi:10.1016/j.mito.2017.07.004

75. Zhang M, Zhou X, Li C, et al. Mitochondrial haplogroup M9a specific variant ND1 T3394C may have a modifying role in the phenotypic expression of the LHON-associated ND4 G11778A mutation. *Mol Genet Metab*. 2010;101(2-3):192-199. doi:10.1016/J.YMGME.2010.07.014

76. Ji F, Sharpley MS, Derbeneva O, et al. Mitochondrial DNA variant associated with Leber hereditary optic neuropathy and high-altitude Tibetans. *Proc Natl Acad Sci U S A*. 2012;109(19):7391-7396. doi:10.1073/PNAS.1202484109/-/DCSUPPLEMENTAL/PNAS.201202484SI.PDF

77. Baranowska E, Niedzwiecka K, Panja C, et al. Probing the pathogenicity of patient-derived variants of MT-ATP6 in yeast. *Dis Model Mech*. 2023;16(4):dmm049783. doi:10.1242/DMM.049783

78. Lamminen T, Majander A, Juvonen V, et al. A mitochondrial mutation at nt 9101 in the ATP synthase 6 gene associated with deficient oxidative phosphorylation in a family with Leber hereditary optic neuroretinopathy. *Am J Hum Genet*. 1995;56(5):1238. Accessed March 13, 2025. https://pmc.ncbi.nlm.nih.gov/articles/PMC1801467/

79. Erb M, Hoffmann-Enger B, Deppe H, et al. Features of idebenone and related short-chain quinones that rescue ATP levels under conditions of impaired mitochondrial complex I. *PLoS One*. 2012;7(4). doi:10.1371/JOURNAL.PONE.0036153

Figure legends

Figure 1 Family trees. For each available individual the mutated (m) and wild-type (+) alleles are reported. The wild-type Y chromosome (y) is reported when the mutated allele is on X chromosome in males.

Figure 2 Illustrative findings in eye and brain imaging. (A) OCT of both eyes (OO) from Family D, patient II:1 and (B) OCT with RGC analysis of OO from Family R, Patient II:1. Both cases show bilateral diffuse optic nerve atrophy with partial sparing of nasal quadrant. (C) Axial and (D) coronal T2-wi sequences from Family R, Patient II:1, showing hyperintensities, initial atrophy and vacuolar degeneration of putamen and hyperintensity of caudati. (E) and (F) coronal long TR sequences from Family H, Patient II:1, showing bilateral pallidal and dentati hyperintensity.

Figure 3 Core subunits' missense variants modeling. (A) Localization in the CI structure of the core subunits considered in this work. CI is shown in ribbons colored in grey, while the NDUFS7, NDUFV1, and NDUFV2 subunits are shown in yellow green, light blue, and indigo, respectively. Co-factors found in the structure are shown as "balls-and-sticks", colored according to the atom type. The remaining panels show the position of the variants described for NDUFS7 **(B)**, NDUFV1 **(C)** and NDUFV2 **(D)** subunits. The residues subject to a variation are shown in "spheres", colored as they are described in the literature (dark cyan), in this work (purple), or in both cases (dark green).

Figure 4 Accessory subunits' missense variants modeling. (A) Localization in the CI structure of the accessory subunits considered in this work. CI is shown in ribbons colored in grey, while

the NDUFA1, NDUFA10, and NDUFB11 subunits are shown in orange, red and yellow, respectively. Co-factors found in the structure are shown in "balls-and-sticks", colored according to atom type. The remaining panels show the position of the variants described for NDUFA1 **(B)**, NDUFA10 **(C)** and NDUFB11 **(D)** subunits. The residues subject to a variation are shown in "spheres", colored as they are described in the literature (dark cyan), in this work (purple), or in both cases (dark green).

Figure 5 Assembly factors' missense variants modeling. The position of the variants described for NDUFAF2 (A), NDUFAF3 (B), NDUFAF4 (C), and NDUFAF8 (D) subunits are shown on the AlphaFold 3 model structures. The residues subject to a variation are shown in "spheres", colored as they are described in the literature (dark cyan) or in this work (purple). Ribbons are colored according to the AlphaFold 3 predicted local distance difference test confidence score (plDDT).

Table 1 Genetic variants details

Family	Individuals	Optic atrophy	Gene	Subunit type, location (module)	Inheritance	Gene MIM#	Genotype	Protein
A	II-1	Plus	*NDUFS7*	Core, peripheral arm (Q)	AR	601825	NM_024407.5:c.[223C>T];[559_564delinsTAGAT]	NP_077718.3:p.[(Arg75Cys)];[(Ala187*)]
B	II-2	Isolated	*NDUFS7*	Core, peripheral arm (Q)	AR	601825	NM_024407.5:c.[298C>T];[298C>T]	NP_077718.3:p.[(Arg100Cys)];[(Arg100Cys)]
C	III-1	Isolated	*NDUFS7*	Core, peripheral arm (Q)	AR	601825	NM_024407.5:c.[298C>T];[298C>T]	NP_077718.3:p.[(Arg100Cys)];[(Arg100Cys)]
D	II-1, II-2	Isolated	*NDUFS7*	Core, peripheral arm (Q)	AR	601825	NM_024407.5:c.[313C>T];[313C>T]	NP_077718.3:p.[(Arg105Cys)];[(Arg105Cys)]
E	II-1	Plus	*NDUFS7*	Core, peripheral arm (Q)	AR	601825	NM_024407.5:c.[313C>T];[313C>T]	NP_077718.3:p.[(Arg105Cys)];[(Arg105Cys)]
F	III-2	Isolated	*NDUFV1*	Core, peripheral arm (Q)	AR	161015	NM_007103.4:c.[1156C>A];[1156C>A]	NP_009034.2:p.[(Arg386Ser)];[(Arg386Ser)]
G	II-1	Isolated	*NDUFV2*	Core, peripheral arm (Q)	AR	600532	NM_021074.5:c.[163T>G];[674G>A]	NP_066552.2:p.[(Phe55Val)];[(Cys225Tyr)]
H	II-1	LLS	*NDUFA1*	Accessory, membrane arm (P_P)	XLR	300078	NM_004541.4:c.[28T>C];[0]	NP_004532.1:p.[(Ser10Pro)];[0]
I	II-1	Plus	*NDUFA1*	Accessory, membrane arm (P_P)	XLR	300078	NM_004541.4:c.[28T>C];[0]	NP_004532.1:p.[(Ser10Pro)];[0]
J	II-1	Plus	*NDUFA1*	Accessory, membrane arm (P_P)	XLR	300078	NM_004541.4:c.[55C>T];[0]	NP_004532.1:p.[(Pro19Ser)];[0]
K	II-1	Plus	*NDUFA10*	Accessory, membrane arm (P_P)	AR	603835	NM_004544.4:c.[233_235del];[233_235del]	NP_004535.1:p.[(Ala78del)];[(Ala78del)]
L	II-1	Plus	*NDUFA10*	Accessory, membrane arm (P_P)	AR	603835	NM_004544.4:c.[233_235del];[233_235del]	NP_004535.1:p.[(Ala78del)];[(Ala78del)]
M	II-2, II-3	Isolated	*NDUFA10*	Accessory, membrane arm (P_P)	AR	603835	NM_004544.4:c.[1009C>T];[1009C>T]	NP_004535.1:[(p.Arg337Cys)];[(p.Arg337Cys)]
N	II-1, II-2	Isolated	*NDUFA12*	Accessory, peripheral arm (N/Q interface)	AR	614530	NM_018838.5:c.[69T>G];[69T>G]	NP_061326.1:p.[(Tyr23*)];[(Tyr23*)]
O	II-1	Plus	*NDUFB11*	Accessory, membrane arm (P_D)	XLR	300403	NM_019056.7:c.[276_278del];[0]	NP_061929.2:p.[(Phe93del)];[0]
P	II-2, II-4	Plus	*NDUFAF2*	Assembly, peripheral arm (N/Q interface)	AR	609653	NM_174889.5:c.[95A>G];[148del]	NP_777549.1:p.[(Tyr32Cys)];[(Arg50Glufs*3)]
Q	II-1	Plus	*NDUFAF2*	Assembly, peripheral arm (N/Q interface)	AR	609653	NM_174889.5:c.[114C>G];[114C>G]	NP_777549.1:p.[(Tyr38*)];[(Tyr38*)]
R	II-1	LLS	*NDUFAF3*	Assembly, peripheral arm (Q)	AR	612911	NM_199069.2c.[5C>A];[489_490del]	NP_951032.1:p.[(Ala2Asp)];[(Gly164Serfs*29)]
S	II-1	Isolated	*NDUFAF4*	Assembly, peripheral arm (Q)	AR	611776	NM_014165.4:c.[224del];[413T>C]	NP_054884.1p.[(Pro75Leufs*7)];[(Ile138Thr)]
T	II-2, II-3	Isolated	*NDUFAF4*	Assembly, peripheral arm (Q)	AR	611776	NM_014165.4:c.[413T>C];[413T>C]	NP_054884.1:p.[(Ile138Thr)];[(Ile138Thr)]
U	II-1, II-2	Isolated	*NDUFAF8*	Assembly, peripheral arm (Q)	AR	618461	NM_001086521.2:c.[44T>G];[44T>G]	NP_001079990.1:p.[(Leu15Arg)];[(Leu15Arg)]
V	II-1, II-2, II-3	Plus, Isolated	*NDUFAF8*	Assembly, peripheral arm (Q)	AR	618461	NM_001086521.2:c.[195+271C>T];[195+271C>T]	NP_001079990.1:p.?
W	II-2	Isolated	*NDUFAF8*	Assembly, peripheral arm (Q)	AR	618461	NM_001086521.2:c.[195+271C>T];[195+271C>T]	NP_001079990.1:p.?

1

2 **Table 2 Clinical features**

Family: ID	Optic atrophy		Other symptoms	MRI findings
	Type of onset	AOO, years		
A: II-1	LHON-like	16	Upbeat nystagmus	Optic nerve atrophy, new tiny focus of T2/FLAIR signal abnormality in the left cerebral peduncle
B: II-2	LHON-like	25	-	Optic nerve atrophy
C: III-1	Insidious	9–10	Neurogenic bladder	N/A
D: II-1	Insidious	2–6	-	MRI normal
D: II-2	Insidious	2–3	-	MRI normal
E: II-1	LHON-like	10	Wolff-Parkinson-White syndrome	MRI normal
F: III-2	LHON-like	16	-	MRI normal
G: II-1	Insidious	2–12	Hyperintensity of MRI T2 signal of the spinal cord, Vitamin B12 deficiency	Hyperintensity of the posterior part of the cervical spinal cord
H: II-1	Insidious	2	Pendular nystagmus, Abnormal basal ganglia MRI signal intensity, elayed ability to walk	Bilateral pallidal and dentati hyperintensity in TR sequences
I: II-1	Insidious	3	Mild neurosensory hearing impairment	Optic nerve atrophy
J: II-1	Insidious	5	Nystagmus, Polyneuropathy, Intellectual disability, borderline, Mild neurosensory hearing impairment, Sensory ataxia	Optic nerve atrophy, very mild atrophy of cerebellar vermis
K: II-1	Insidious	0–1	Multiple sclerosis, Pendular nystagmus, Decreased mean corpuscular volume, CNS demyelination	Demyelinating brain lesions (images and report not available)-2021 (followed elsewhere for MS)
L: II-1	Insidious	5	Cerebellar atrophy, abnormality of extrapyramidal motor function, cerebral cortical atrophy, generalized-onset seizure, intellectual disability, borderline, mild neurosensory hearing impairment, cognitive impairment	Cerebellar and mild cerebral cortical atrophy
M: II-2	Insidious	2–12	-	MRI normal
M: II-3	Insidious	2–12	-	MRI normal
N: II-2	LHON-like	15	-	MRI normal
N: II-3	LHON-like	16	-	MRI normal
O: II-1	Insidious	0–1	Megaloblastic anaemia, abnormality of the gallbladder, folate deficiency	Optic nerve atrophy
P: II-2	Insidious	6–12	Cerebral calcification, lactic acidosis, sensory axonal neuropathy, mild neurosensory hearing impairment, hyperintensity of cerebral white matter on MRI, multiple meningiomas, vitamin B_{12} deficiency	Brainstem white matter changes; multiple frontal and falx calcified meningiomas; optic nerve atrophy; abnormal lactic acid accumulation at MRS
P: II-4	Insidious	2–6	Lactic acidosis, Sensory axonal neuropathy, Cerebral aneurysm, Abnormal basal ganglia MRI signal intensity	Focal left substantia nigra hyperintensity; left M1 aneurysm; optic nerve atrophy
Q: II-1	LHON-like	2–6	Nystagmus, Peripheral axonal neuropathy	MRI normal
R: II-1	Insidious	0–3	Motor delay, Abnormal basal ganglia MRI signal intensity	Bilateral striatal necrosis (putaminal bilateral hyperintensity)
S: II-1	Insidious + LHON-like	0–3	-	MRI normal
T: II-2	Insidious	3	-	Mild disproportionate volume loss involving the superior vermis and cerebellar hemispheres noticed.
T: II-3	Insidious	5	-	Mild disproportionate volume loss involving the superior vermis and cerebellar hemispheres noticed.
U: II-1	LHON-like	10	-	MRI normal
U: II-2	LHON-like	13	-	MRI normal
V: II-1	LHON-like	3	Strabismus, hyperopia, nystagmus, unsteady gait, mild developmental delay	Non-specific white matter lesions
V: II-2	LHON-like	3	Strabismus, hyperopia	Non-specific white matter lesions

V: II-3	LHON-like	4	Strabismus, hyperopia	Non-specific white matter lesions
W: II-2	Insidious	0–1	-	MRI normal

ID = Individual; OD = right eye; OS = left eye; OOA = age of onset; N/A, not available; ONH = optic nerve head.

Table 3 Ophthalmic findings

Family	ID	Age at last visit (years)	Fundus oculi description	VA OD	VA OS	OCT RNFL avg OD	OCT RNFL avg OS	Visual field MD OD	Visual field MD OS
A	II-1	30	Bilateral and symmetrical optic atrophy	0.01	0.01	56	55	-27.74	-30.84
B	II-2	39	Temporal optic nerve pallor	1	0.6	N/Q, diffuse thinning more pronounced in temporal quadrant		N/A	N/A
C	III-1	25	Bilateral OA, High myopia	0.8	0.4	47	54	-7.23	-9.12
D	II-1	7	Temporal optic nerve pallor	0.8	0.4	49	44	N/A	N/A
D	II-2	5	Temporal optic nerve pallor	0.6	0.9	42	43	N/A	N/A
E	II-1	30	Diffuse optic atrophy	0.05	0.05	N/A	N/A	N/Q, cecocentral scotoma	
F	III-2	27	Bilateral OA	0.01	0.01	55	46	N/A	N/A
G	II-1	20	Diffuse optic nerve pallor more evident temporally, small ONH	0.1	0.1	46	48	-14.65	-10.92
H	II-1	22	Pale optic disk temporal bilaterally	0.4	0.3/0.4	N/A	N/A	N/A	N/A
I	II-1	17	Temporal optic nerve pallor	0.15	0.1	N/A	N/A	N/A	N/A
J	II-1	45	Optic nerve pallor (OS>OD)	0.02	0.02	N/Q, inside normal values		N/Q, central scotoma and enlargement of the blind spot	
K	II-1	37	Diffuse optic nerve pallor	0.1	0.16	N/Q	N/Q	-14.25	-16.6
L	II-1	35	N/A (uncooperative patient)	N/A	N/A	N/A	N/A	N/A	N/A
M	II-2	18	Temporal optic nerve pallor	0.25	0.16	65	64	-2.82[a]	-6.56[a]
M	II-3	16	Temporal optic nerve pallor	0.4	0.5	58	56	-3.69[a]	-3.66[a]
N	II-2	24	Bilateral OA, marked loss of papillo-macular bundle	0.01	0.01	N/A	N/A	N/Q, generalized depression	
N	II-3	18	OD severe OA, OS some preservation of nasal side	0.01	0.02	N/A	N/A	N/A	N/A
O	II-1	25	Temporal pallor	0.32	0.4	67	68	-10.2	-8.25
P	II-2	52	Diffuse optic nerve pallor more evident temporally	0.25	0.2	41	39	-12.63	-12.73
P	II-4	37	Diffuse optic nerve pallor more evident temporally	0.13	0.1	43	37	-16.43	-19.41
Q	II-1	15	Bilateral OA	0.16	0.01	40	43	-20.54	-11.98
R	II-1	7	ONH pallor	0.5	0.3	38	41	N/A	N/A
S	II-1	18	Temporal pallor followed by diffuse pallor after recurrence	0.2	0.25	42	41	-30.08	-32.00
T	II-2	17	Bilateral OA, Left Coats disease	0.5	0.5	56	55	N/A	N/A
T	II-3	13	Bilateral OA	1	1	68	58	-6.64	-13.05
U	II-1	24	N/A	0.015	0.03	40	55	N/A	N/A
U	II-2	N/A	N/A	N/A	N/A	N/A	N/A	N/A	N/A
V	II-1	15	Bilateral OA, Tortuous vessels	0.03	0.03	N/Q	N/Q	-24.76	-20.78
V	II-2	11	Bilateral OA, Tortuous vessels	0.08	0.063	N/Q	N/Q	-6.21	-6.77
V	II-3	6	Bilateral OA, Tortuous vessels	0.063	0.063	N/A	N/A	N/A	N/A
W	II-2	54	Bilateral OA	0.08	0.05	40	43	N/A	N/A

ID, Individual; VA, visual acuity; OD, right eye; OS, left eye; N/A, not available; N/Q, not quantificable; OCT, optical coherence tomography; RNFL, retinal nerve fiber layer; MD, mean deviation.
[a]Visual field test with M-700, Medmont International, Vermont, Australia.

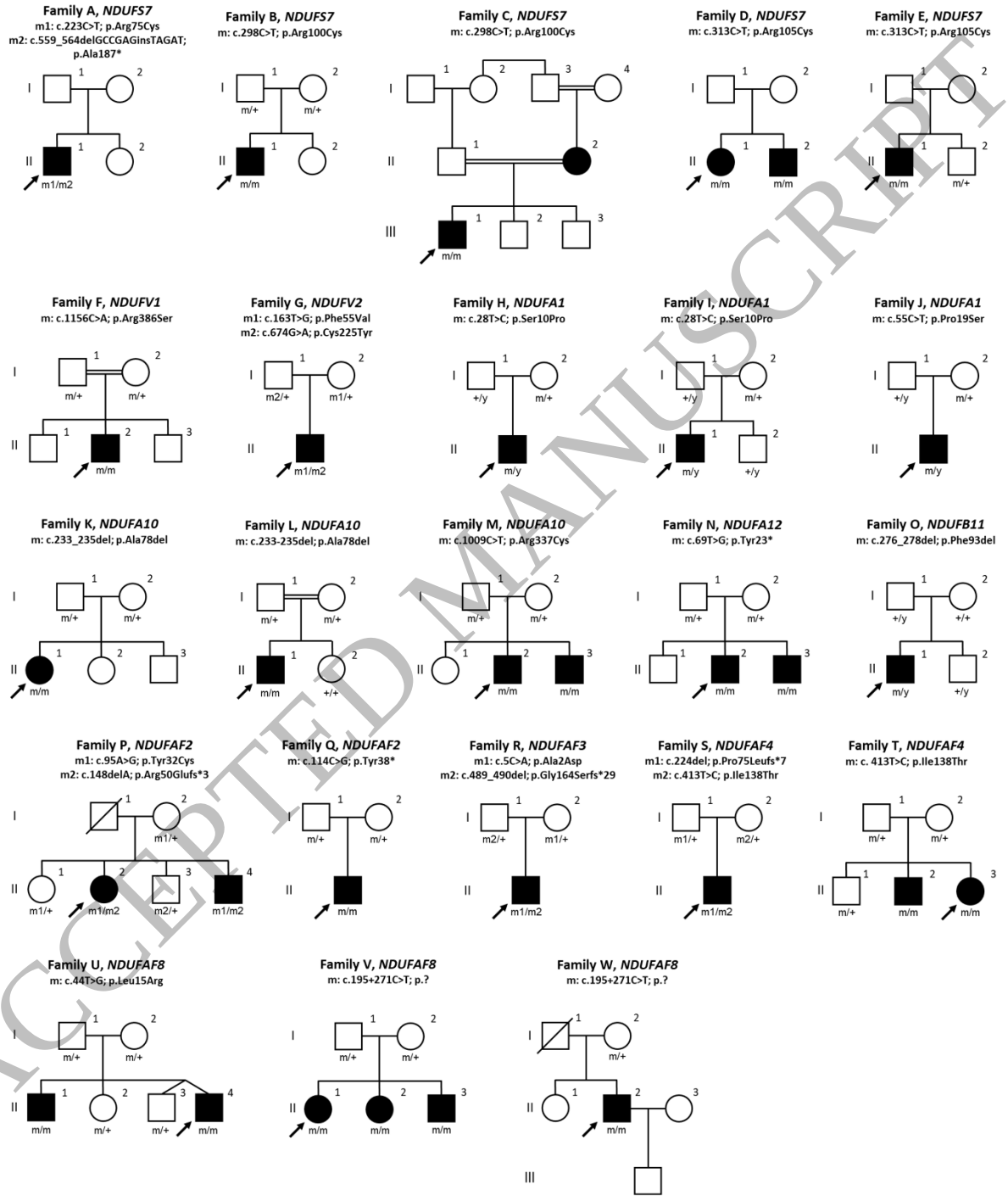

Figure 1
157x189 mm (DPI)

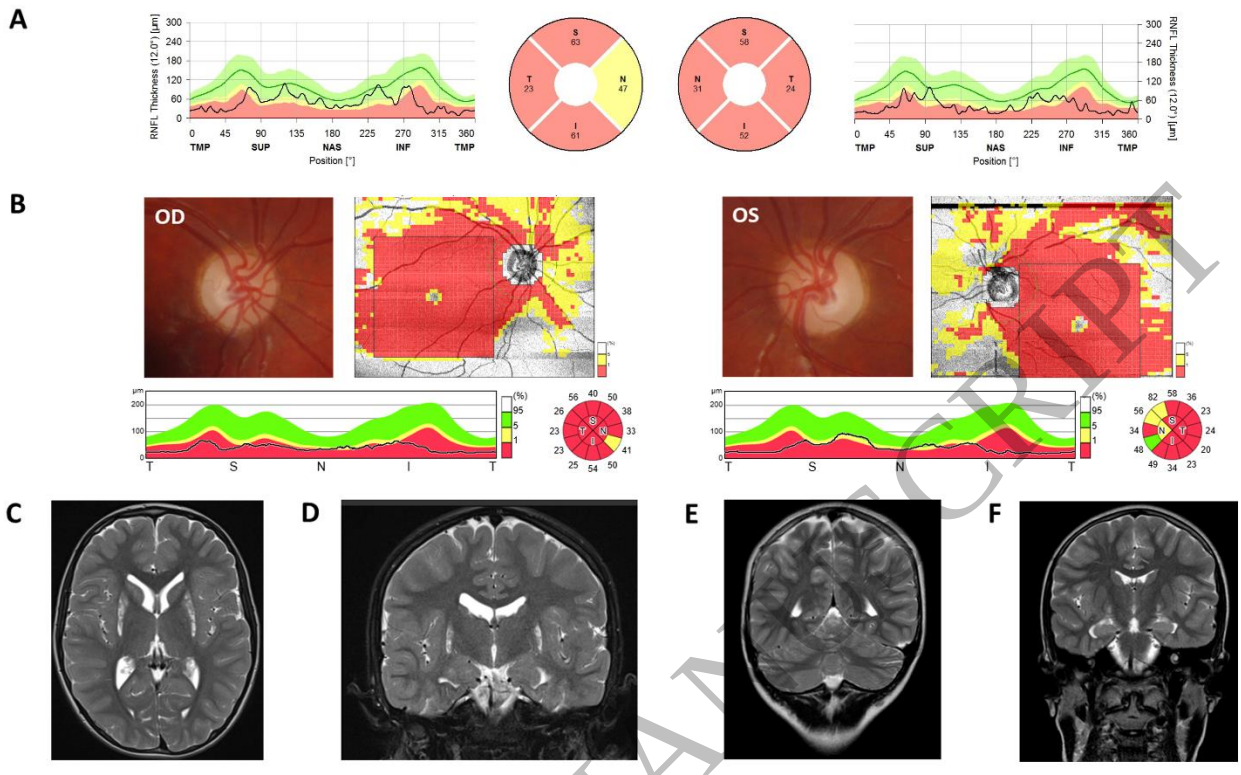

Figure 2
165x102 mm (DPI)

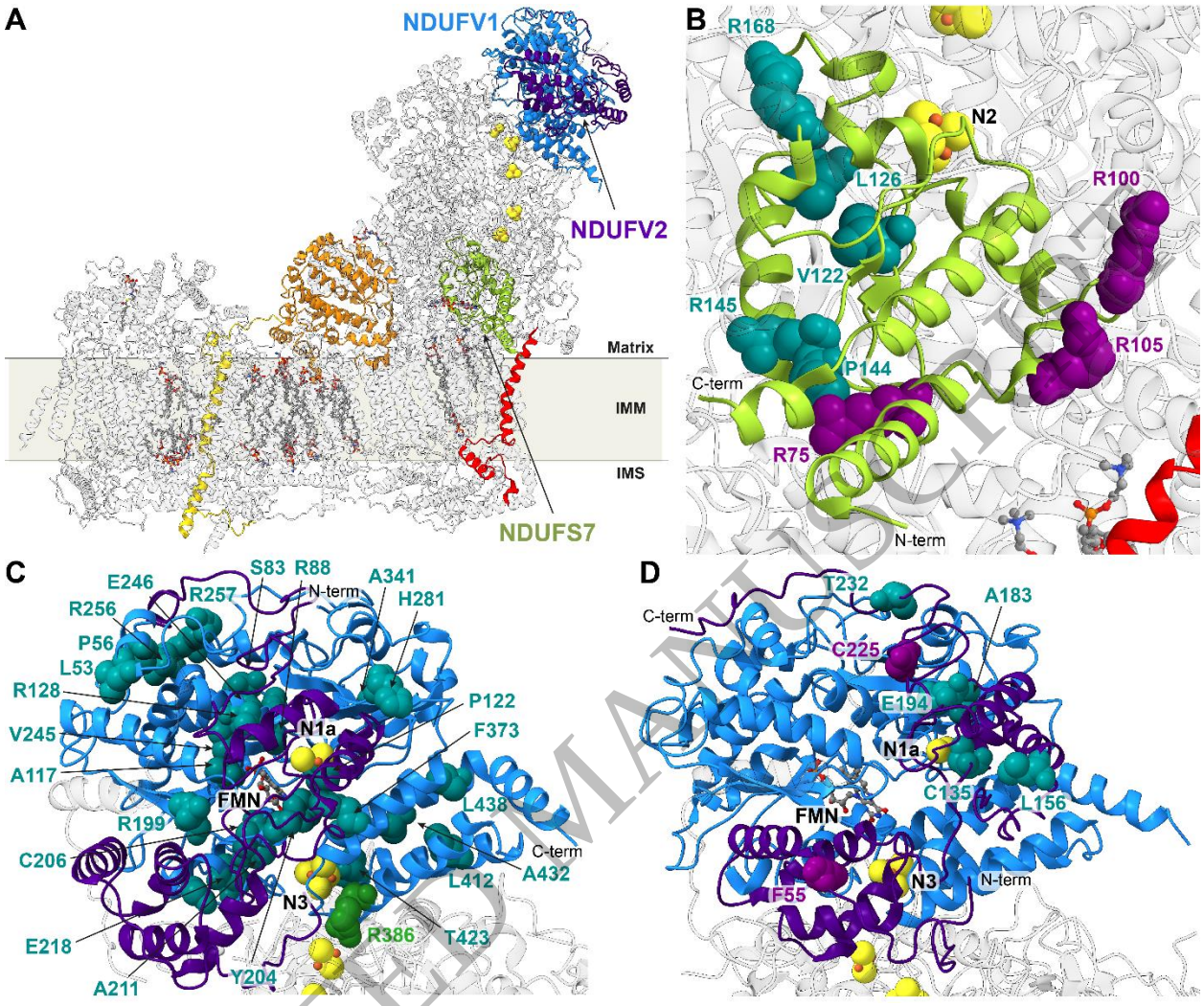

Figure 3
165x138 mm (DPI)

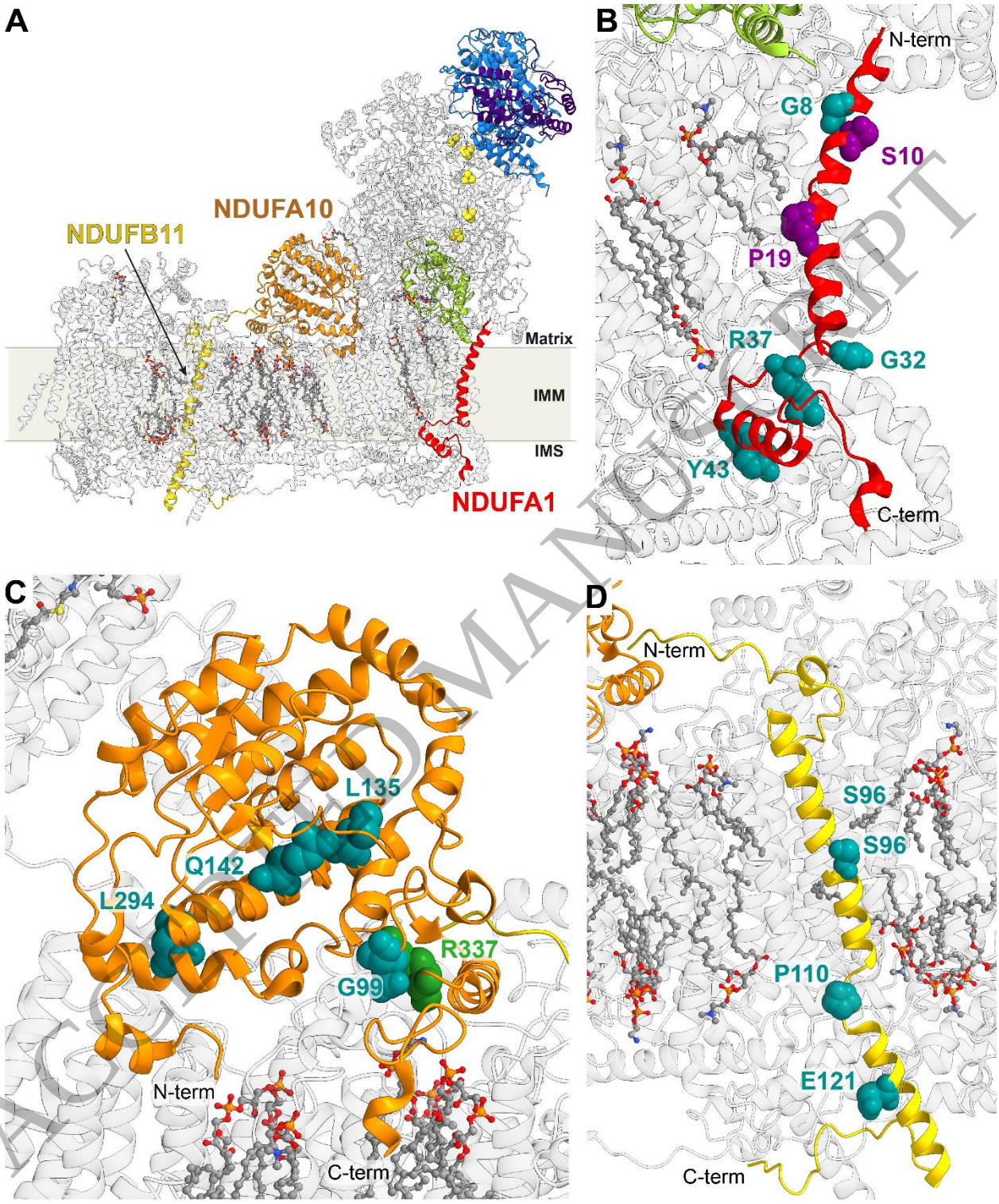

Figure 4
165x199 mm (DPI)

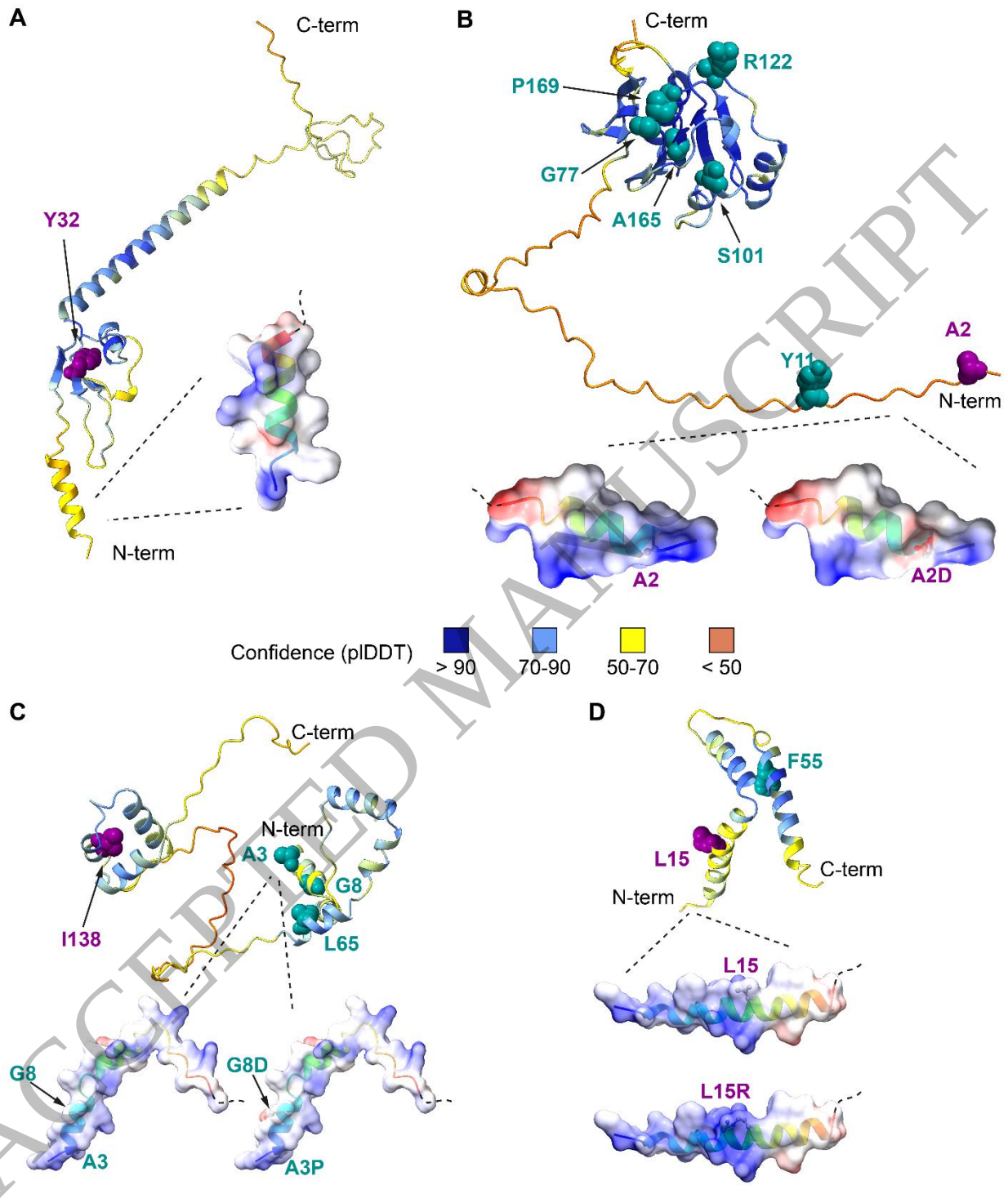

Figure 5
165x195 mm (DPI)